Strong coupling of different cavity modes in photonic molecules formed by two adjacent microdisk microcavities

Hsuan Lin,[1] Jhih-Hao Chen,[1] Shih-Shing Chao,[1] Ming-Cheng Lo,[2] Sheng-Di Lin,[2] and Wen-Hao Chang[1,*]

[1]*Department of Electrophysics, National Chiao Tung University, Hsinchu 300, Taiwan*
[2]*Department of Electronics Engineering, National Chiao Tung University, Hsinchu 300, Taiwan*
**whchang@mail.nctu.edu.tw*

Abstract: Strong couplings between cavity modes in photonic molecules formed by two preselected nearly identical microdisk microcavities with embedded quantum dots are investigated. By continuously tuning the refractive index of one microdisk, clear anticrossings in the resonant peak energies associated with crossings in the peak linewidths can be observed. The coupling strengths are extracted by the coupled mode theory and analyzed by the model considering the effective potential confining the electromagnetic waves in the microcavities.

OCIS codes: (230.4555) Coupled resonators; (350.3950) Micro-optics.

References and links

1. T. Yoshie, A. Scherer, J. Hendrickson, G. Khitrova, H. M. Gibbs, G. Rupper, C. Ell, O. B. Shchekin, and D. G. Deppe, "Vacuum Rabi splitting with a single quantum dot in a photonic crystal nanocavity," Nature **432**(7014), 200–203 (2004).
2. J. P. Reithmaier, G. Sęk, A. Löffler, C. Hofmann, S. Kuhn, S. Reitzenstein, L. V. Keldysh, V. D. Kulakovskii, T. L. Reinecke, and A. Forchel, "Strong coupling in a single quantum dot-semiconductor microcavity system," Nature **432**(7014), 197–200 (2004).
3. P. Michler, A. Kiraz, C. Becher, W. V. Schoenfeld, P. M. Petroff, L. Zhang, E. Hu, and A. Imamoğlu, "A quantum dot single-photon turnstile device," Science **290**(5500), 2282–2285 (2000).
4. M. Pelton, C. Santori, J. Vučković, B. Zhang, G. Solomon, J. Plant, and Y. Yamamoto, "Efficient Source of Single Photons: A Single Quantum Dot in a Micropost Microcavity," Phys. Rev. Lett. **89**(23), 233602 (2002).
5. W.-H. Chang, W.-Y. Chen, H.-S. Chang, T. P. Hsieh, J. I. Chyi, and T. M. Hsu, "Efficient single photon sources based on quantum dots in photonic crystal nanocavities," Phys. Rev. Lett. **96**(11), 117401 (2006).
6. N. Gisin, G. Ribordy, W. Tittel, and H. Zbinden, "Quantum cryptography," Rev. Mod. Phys. **74**(1), 145–195 (2002).
7. A. Imamoğlu, D. D. Awschalom, G. Burkard, D. P. DiVincenzo, D. Loss, M. Sherwin, and A. Small, "Quantum Information Processing Using Quantum Dot Spins and Cavity QED," Phys. Rev. Lett. **83**(20), 4204–4207 (1999).
8. A. Laucht, J. M. Villas-Bôas, S. Stobbe, N. Hauke, F. Hofbauer, G. Böhm, P. Lodahl, M.-C. Amann, M. Kaniber, and J. J. Finley, "Mutual coupling of two semiconductor quantum dots via an optical nanocavity," Phys. Rev. B **82**(7), 075305 (2010).
9. M. J. Hartmann, F. G. S. L. Brandao, and M. B. Plenio, "Strongly interacting polaritons in coupled arrays of cavities," Nat. Phys. **2**(12), 849–855 (2006).
10. M. Bayer, T. Gutbrod, J. P. Reithmaier, A. Forchel, T. L. Reinecke, P. A. Knipp, A. A. Dremin, and V. D. Kulakovskii, "Optical Modes in Photonic Molecules," Phys. Rev. Lett. **81**(12), 2582–2585 (1998).
11. A. Dousse, J. Suffczyński, A. Beveratos, O. Krebs, A. Lemaître, I. Sagnes, J. Bloch, P. Voisin, and P. Senellart, "Ultrabright source of entangled photon pairs," Nature **466**(7303), 217–220 (2010).
12. J. W. Fleischer, M. Segev, N. K. Efremidis, and D. N. Christodoulides, "Observation of two-dimensional discrete solitons in optically induced nonlinear photonic lattices," Nature **422**(6928), 147–150 (2003).
13. M. Benyoucef, S. Kiravittaya, Y. F. Mei, A. Rastelli, and O. G. Schmidt, "Strongly coupled semiconductor microcavities: A route to couple artificial atoms over micrometric distances," Phys. Rev. B **77**(3), 035108 (2008).
14. A. V. Kavokin, J. J. Baumberg, G. Malpuech, and F. P. Laussy, *Microcavities* (Academic, 2007), pp. 170–173.
15. E. M. Purcell, "Spontaneous emission probabilities at radio frequencies," Phys. Rev. **69**, 681 (1946).
16. S. V. Boriskina, "Coupling of whispering-gallery modes in size-mismatched microdisk photonic molecules," Opt. Lett. **32**(11), 1557–1559 (2007).
17. B. R. Johnson, "Theory of morphology-dependent resonances: shape resonances and width formulas," J. Opt. Soc. Am. A **10**(2), 343 (1993).

#134575 - $15.00 USD Received 7 Sep 2010; revised 23 Oct 2010; accepted 23 Oct 2010; published 29 Oct 2010

18. J. Shainline, S. Elston, Z. Liu, G. Fernandes, R. Zia, and J. Xu, "Subwavelength silicon microcavities," Opt. Express **17**(25), 23323–23331 (2009).

1. Introduction

Semiconductor quantum dots (QDs) coupled to an optical microcavity, known as a cavity quantum electrodynamics (QED) system, have been a research field of intense investigations. It offers a solid-state system not only for exploring the fundamentals of light-matter coupling [1,2], but also for applications in quantum information processing, such as single photon [3–5] sources for quantum cryptography [6]. A solid-state cavity QED system is also promising for quantum computation [7]. Two or more QDs can be coupled to each other via the same cavity field to realize parallel quantum-bit (qbit) operations [7,8]. However, practical implementations of multiple qbits operations remain difficult because of the technical challenges in selective addressing different QDs in a microcavity. Recently, some proposals turn to utilize individual quantum systems in different microcavities that are coupled to each other via the exchange of photons [9], i.e., forming so-called photonic molecules (PM) [10,11] or a photonic lattice [12]. Based on this scheme, addressing individual QDs with optical lasers in separate microcavities becomes easier. However, due to the limited fabrication accuracy and the inhomogeneous QD size distribution, it is still difficult to realize a pair of, or even an array of, coupled QD-cavity systems. More recently, a flexible way for the planar integration of microdisk (MD) microcavities was reported by Benyoucef *et al* [13]. In this scheme, individual MDs are transferred to a sapphire substrate and positioned into PMs by micromanipulations. This approach may practically overcome the difficulties arising from the cavity size and QD size fluctuations, because suitable MDs with QDs can be preselected before positioned into PMs.

In this work, the coupling behaviors of optical modes in PMs formed by two preselected nearly identical MDs are investigated. Strong couplings between whispering-gallery modes (WGMs) with identical or different radial and azimuthal mode numbers are observed, resembling the hybridizations of different atomic orbits in real molecules. By using the coupled mode theory to analyze the anticrossing in resonance frequencies and the crossing in cavity decay rate, the coupling strengths of different modes can be extracted. The observed coupling strengths for different WGMs are explained by the "effective barrier" for the confined optical modes in individual MDs.

2. Sample preparation and experimental setup

The sample was grown on a GaAs substrate by molecular beam epitaxy. It consists of a 600 nm thick $Al_{0.9}Ga_{0.1}As$ sacrificial layer on the substrate, followed by a 200 nm thick GaAs waveguide layer with a layer of InAs self-assembled QDs embedded in the middle. The sample was processed into MDs by using electron-beam lithography. The waveguide layer and the sacrificial layer were etched in a HBr-based etchant. The sacrificial layer underneath the MDs was then completely removed in a buffered oxide etchant, leaving an array of MDs on the GaAs substrate. To provide optical confinements, these MDs were transferred onto a sapphire substrate, using a polymethylmethacrylate (PMMA) layer as glue. These MDs were up-side-down pressed onto the sapphire substrate and baked at 130 °C for 2 minutes. Finally, the PMMA layer was then removed in an acetone solution, leaving MDs on the sapphire substrate. In the final procedure, the acetone solution was diluted properly with isopropyl alcohol. This can reduce the removing rate for the PMMA layer and hence preventing the MDs to flow rapidly away from the sapphire substrate in the solution. By optimizing the removing rate and the immersion time, the PMMA layer can be slowly but completely removed, while keeping about 75% of the MDs residing on the sapphire surface. The high transfer efficiency allows us to assemble PMs from preselected MDs with a higher throughput. Microphotoluminescence (μ-PL) measurements were carried out at room temperature by using either a He-Ne laser or a cw Ti:Sapphire laser as an excitation source. Emission signals were collected from the MD top and analyzed by a 0.5-m spectrometer

#134575 - $15.00 USD Received 7 Sep 2010; revised 23 Oct 2010; accepted 23 Oct 2010; published 29 Oct 2010

equipped with an InGaAs diode array. The optical emissions were collected without spatial filtering, i.e., the emissions from all portions of MDs or PMs were simultaneously detected.

3. Experimental results and discussion

Figure 1(a) shows the μ-PL spectra of two individual MDs. The diameters of the two MDs are about 3.6 μm, which have been determined by scanning electron microscopy (SEM) before transfer onto the sapphire substrate. Several sharp emission lines superimposing on the emission band of InAs QDs can be observed. These sharp lines are WGMs of the MD, which can be classified by transverse-electric-field (TE) modes, $TE_{\ell,m}$, with ℓ and m denoting the radial and the azimuthal mode numbers, respectively. Here we defined the TE mode as an electromagnetic (EM) wave propagating along the disk plane with an electric field perpendicular to the growth direction. To identify the mode numbers of these peaks, three-dimensional finite-difference time-domain (3D-FDTD) calculations considering a 200-nm-thick GaAs MD with a diameter of 3.6 μm on a sapphire substrate have been performed. Our calculations suggest that the peaks shown in Fig. 1(a) are $TE_{2,22}$, $TE_{1,26}$, $TE_{2,21}$, $TE_{1,25}$, $TE_{2,20}$ and $TE_{1,24}$ WGMs. We have also checked the polarization properties of these resonant peaks emitted from the MD edge. We conclude that no transverse-magnetic-field (TM) mode (i.e., with a magnetic field perpendicular to the growth direction) was observed in this spectral range. In fact, our calculations indicate that the MDs also support TM modes. However, since the spectral range investigated here is around the QD ground state, from which the emission is mainly polarized along the disk plane, the corresponding resonant peaks are therefore also dominated by TE modes. In Fig. 1(a), we intentionally select two MDs displaying resonant peaks at nearly identical wavelengths, indicating that the two MDs only have ~0.1% variation

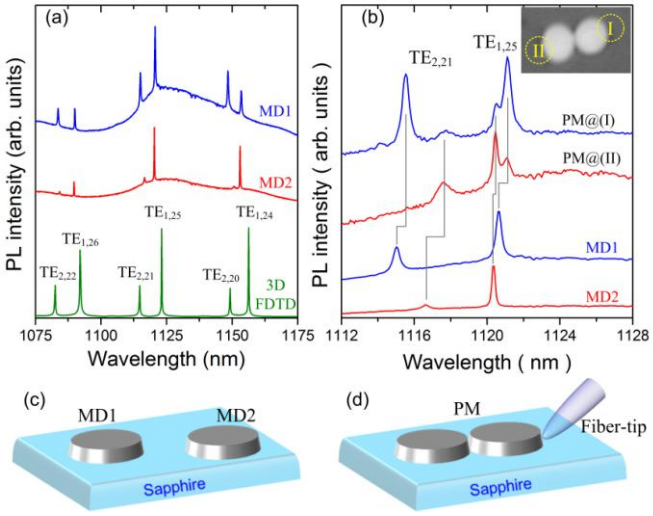

Fig. 1. (a) The micro-PL spectra of two individual MDs (MD1 and MD2). A simulated spectrum obtained from 3D-FDTD calculations is also shown. (b) The micro-PL spectra of MD1 and MD2 near the $TE_{2,21}$ and $TE_{1,25}$ modes before and after the two MDs were positioned to form a PM. The inset shows an image of the PM under an optical microscope.

#134575 - $15.00 USD Received 7 Sep 2010; revised 23 Oct 2010; accepted 23 Oct 2010; published 29 Oct 2010

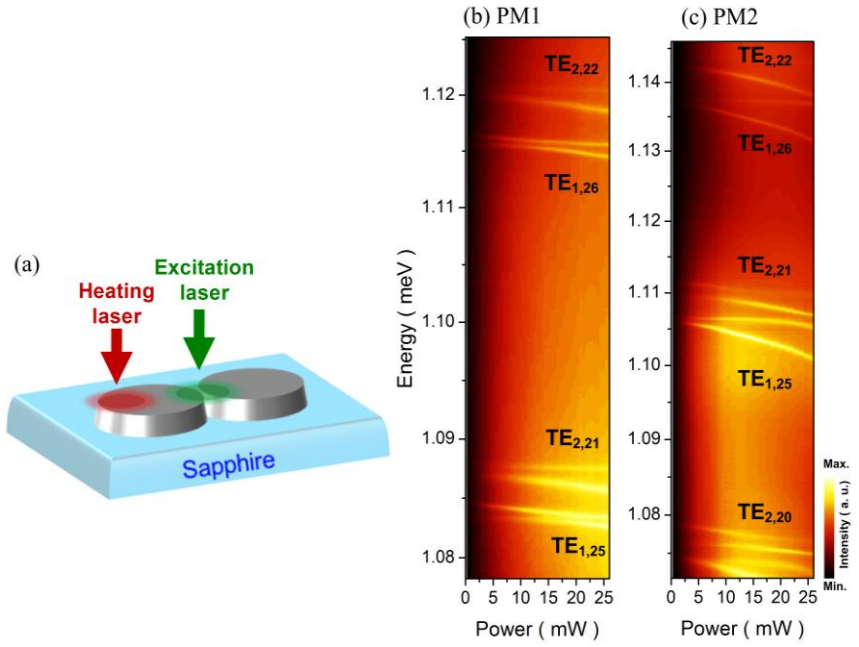

Fig. 2. (a) A schematic for the two-laser scheme used for laser local heating of one MD. (b) and (c) are the micro-PL intensity maps of PM1 and PM2 as a function of the heating laser power.

in diameter. After spectral measurements, the two MDs were positioned into an adjacent pair by using a fiber-tip manipulator, forming a closely spaced PM as shown in the inset of Fig. 1. The μ-PL spectra near the $TE_{1,25}$ and $TE_{2,21}$ WGMs of the two MDs before and after forming a PM are displayed in Fig. 1(b). After the two MDs were positioned together, both the $TE_{1,25}$ and $TE_{2,21}$ modes shift slightly to a longer wavelength, indicative of mode couplings after PM formations.

To control the mode coupling in PMs, we employed a two-laser scheme in our μ-PL measurements, as shown in Fig. 2(a). A first laser beam from a He-Ne laser was focused onto the middle of the two MDs for the excitation of both MDs. A second laser beam from a Ti:Sapphire laser (750 nm), which was off-axis slightly from the first laser beam, was focused onto one of the MDs for laser local heating. Increasing the heating laser power can increase the refractive index of one MD, and thereby the WGMs can be brought into exact resonance even though they are detuned slightly from one another before forming a PM. Figure 2(b) and 2(c) show the contour plots of the PL intensity maps for two different PMs as a function of the heating laser power. Each WGM shows a pair of lines from different MDs, of which only the smaller MD was heated by the Ti:Sapphire laser [see Fig. 2(a)]. Some WGM pairs with larger initial detuning, such as the $TE_{1,25}$ and $TE_{1,26}$ modes of PM1, can be brought into resonance by the laser heating. A clear anticrossing with a minimal energy splitting can be observed at a certain heating power, indicative of a strong coupling between the WGM pair. However, for some WGM pairs with smaller initial detuning, (e.g., $TE_{2,21}$ in PM1 or $TE_{1,26}$ in PM2), their energy splittings become even larger with the increasing laser power, indicating that these WGM pairs are brought away from resonance by the laser heating. We noted that the heating induced energy shifts in PM1 and PM2 are not identical. This may arise from the different thermal contacts of the MDs with the sapphire substrate.

The mode coupling in a PM can be described by the coupled mode theory. The eigenfrequencies of coupled modes ω_+ and ω_- are given by

#134575 - $15.00 USD Received 7 Sep 2010; revised 23 Oct 2010; accepted 23 Oct 2010; published 29 Oct 2010

$$\omega_{\pm} = \frac{\omega_1 + \omega_2}{2} - i\frac{\gamma_1 + \gamma_2}{4} \pm \sqrt{g^2 - \frac{[(\gamma_1 - \gamma_2) + 2i(\omega_1 - \omega_2)]^2}{16}}, \quad (1)$$

where $\omega_{1,2}$ and $\gamma_{1,2}$ are the frequencies and damping rates of WGMs in uncoupled MD1 and MD2, respectively; and g represents the coupling strength between the two MDs. From Eq. (1), the energies $E_{\pm}$ and linewidths $\Gamma_{\pm}$ of coupled WGMs can be obtained from the real part and the imaginary part of $\hbar\omega_{\pm}$, respectively. According to the sign of the expression under the square root at zero detuning ($\omega_1 = \omega_2$) determined by g and $\gamma_{1,2}$, the coupling behaviors can be divided into two regimes: the *strong* and the *weak* coupling regimes. If $g > |\gamma_1 - \gamma_2|/4$, $\omega_{\pm}$ exhibits normal mode splitting at $\omega_1 = \omega_2$, corresponding to the strong coupling regime, where the cavity photons can coherently transfer between the two MDs before leaking irreversibly into the free space [14]. Conversely, if $g < |\gamma_1 - \gamma_2|/4$, the square root in Eq. (1) becomes imaginary at $\omega_1 = \omega_2$, so that the energy splitting disappears. This corresponds to the weak coupling regime, where the damping rates of the two MDs will be modified when they are on exact resonance [15].

In order to make a direct comparison of Eq. (1) with our experimental results, we use the relation $E_1(P) = E_1(0) + \alpha P + \beta P^2$ to describe the energy shift of each mode as a function of laser power P on one MD, where α and β are treated as fitting parameters in our analysis. Figure 3 displays the peak energies of the

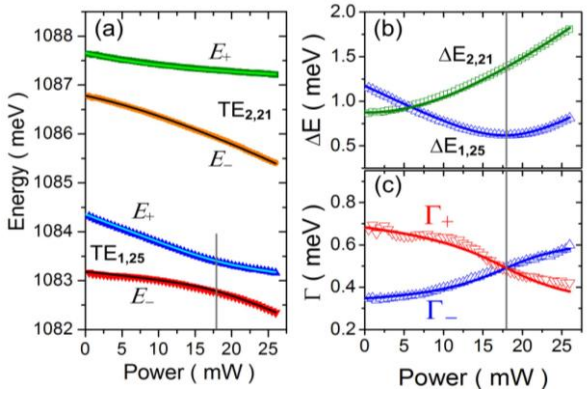

Fig. 3. (a) The peak energies of the upper and lower branches of the $TE_{2,21}$ and $TE_{1,25}$ WGMs in PM1 as a function of the heating laser power. (b) The corresponding energy difference between $TE_{2,21}$ pair and $TE_{1,25}$ pair ($\Delta E_{2,21}$ and $\Delta E_{1,25}$ respectively). (c) The evolution of the linewidths of the upper and lower branches of the $TE_{1,25}$ mode with the heating laser power.

#134575 - $15.00 USD Received 7 Sep 2010; revised 23 Oct 2010; accepted 23 Oct 2010; published 29 Oct 2010

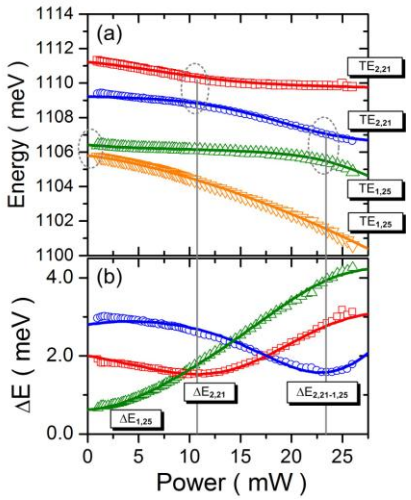

Fig. 4. (a) The evolutions of the peak energies of the $TE_{2,21}$ and $TE_{1,25}$ modes of PM1 with the heating laser power. (b) The corresponding energy differences between the $TE_{2,21}$ pair, $TE_{1,25}$ pair and between the $TE_{1,25}$-$TE_{2,21}$ pair ($\Delta E_{2,21}$, $\Delta E_{1,25}$ and $\Delta E_{2,21\text{-}1,25}$ respectively) as a function of heating laser power.

$TE_{2,21}$ and $TE_{1,25}$ WGMs of PM1 as a function of P. Lines are the best fitting curves obtained from Eq. (1). A clear anticrossing in the $TE_{1,25}$ WGM pair is observed at $P = 18$ mW, indicating that at which the $TE_{1,25}$ modes of the two MDs are on exact resonance (i.e., $\omega_1 = \omega_2$). The exact resonance can be confirmed by the energy splitting between the E_+ and E_- branches of the $TE_{1,25}$ mode, which also goes through a minimum of $\Delta E_{1,25} = 0.62$ meV at 18 mW [Fig. 3(b)]. For the $TE_{2,21}$ WGM pair, a minimum splitting of $\Delta E_{2,21} = 0.8$ meV was observed at $P \approx 0$, indicating that they are already strongly coupled in the beginning. Apart from the energy splitting, we also observe a crossing in linewidths when two WGMs are on resonance. This behavior is illustrated in Fig. 3(c), where the linewidths of the $TE_{1,25}$ WGM pair also exhibit a crossing at 18 mW, in agreement with the behavior predicted by Eq. (1). From the fittings of the energy anticrossing and the linewidth crossing, we can determine the coupling strengths, which are $\hbar g_{1,25} = 0.32$ meV and $\hbar g_{2,21} = 0.45$ meV for the $TE_{1,25}$ and $TE_{2,21}$ modes, respectively. It is worth to mention that the deduced coupling strengths are not equal to half of the measured energy splitting at exact resonance. From Eq. (1), one can see that when $\omega_1 = \omega_2$, the normal splitting is not equal to $2g$ because of in general $\gamma_1 \neq \gamma_2$. Although we used a number of parameters in curve fittings, the estimated coupling strengths are still very rigid. Since the value of $\hbar g$ is mainly influenced by the uncertainties in determining $\hbar\gamma_1$ and $\hbar\gamma_2$, the uncertainty in $\hbar g$ will be small when ΔE is quite larger than $\hbar(\gamma_1 - \gamma_2)/2$.

In Fig. 4, the evolutions of the $TE_{2,21}$ and $TE_{1,25}$ WGMs of PM2 are displayed. Both modes show an anticrossing, which is similar to the coupling behaviors observed in PM1, except for the different coupling strengths and the required heating powers for exact resonance due to the different inter-gap distances and thermal contacts with the substrate. The most interesting feature in Fig. 4 is that the upper branch of $TE_{1,25}$ and the lower branch of $TE_{2,21}$ also exhibit an anticrossing at $P = 23$ mW. This indicates that strong coupling can also occur between different WGMs. By using a four-coupled-mode equation to analyze the data, the coupling strengths can be determined, which are $\hbar g_{1,25} = 0.45$ meV, $\hbar g_{2,21} = 0.86$ meV and $\hbar g_{1,25-2,21} = 0.76$ meV for the $TE_{1,25}$, the $TE_{2,21}$ and that between $TE_{1,25}$ and $TE_{2,21}$ modes, respectively.

#134575 - $15.00 USD Received 7 Sep 2010; revised 23 Oct 2010; accepted 23 Oct 2010; published 29 Oct 2010

From our measurements, we found that the coupling strengths of the second-order radial modes ($\ell = 2$) are larger than that of the adjacent first-order radial modes ($\ell = 1$). However, in Ref. 11 the second-order radial modes were found to have smaller energy splitting at resonant point. To have a better understanding about the coupling strengths of each WGM, 2D FDTD calculations considering a PM formed by two identical MDs with 3.6 μm diameters and an inter-gap of 75 nm have been performed. Here, the inter-gap is treated as an adjustable fitting parameter. The calculated energy splitting for the $TE_{1,25}$, $TE_{2,21}$, $TE_{1,26}$ and $TE_{2,22}$ are summarized in Fig. 5. Indeed, we found that the second-order radial modes have larger energy splittings, in consistence with our measurements.

The coupling strength is determined by the overlap between the evanescent waves leak out of the two MDs at the gap. Therefore, to have a detailed understanding of the coupling strength, it is necessary to know the factors controlling the field intensity of each mode decaying into the free space. Instead of using numerical simulations [16], in the following we analyze the field decay in an analytical way, which can give insight into the key factor controlling the coupling strength.

Let us consider a homogeneous MD with refractive index $n = n_0$ and radius a in free space ($n = 1$). The wave equation for the field inside and outside the MD can be decomposed into an azimuthal part and a radial part. For the WGM with mode numbers (ℓ, m), the radial equation for the field amplitude $R_\ell(r)$ is given by [17,18]

$$\frac{1}{r}\frac{d}{dr}[r\frac{d}{dr}R_\ell(r)] + (k_m^2 n_{\text{eff}}^2 - \frac{m^2}{r^2})R_\ell(r) = 0, \tag{2}$$

where k_m is the wave vector and n_{eff} is the effective refractive index, which is a function of r and λ_m (the resonant wavelength of the m^{th} mode). If we introduce an "effective potential",

$$V_{\text{eff}}(r) = k_m{}^2(1 - n_{\text{eff}}^2) + \frac{m^2}{r^2}, \tag{3}$$

and an "effective energy" $E_{\text{eff}} = k_m^2$ for the field, then Eq. (2) can be rewritten as the form of a Schrödinger-like equation:

$$-\frac{1}{r}\frac{d}{dr}[r\frac{d}{dr}R_\ell(r)] + V_{\text{eff}}(r)R(r) = E_{\text{eff}}R_\ell(r). \tag{4}$$

#134575 - $15.00 USD Received 7 Sep 2010; revised 23 Oct 2010; accepted 23 Oct 2010; published 29 Oct 2010

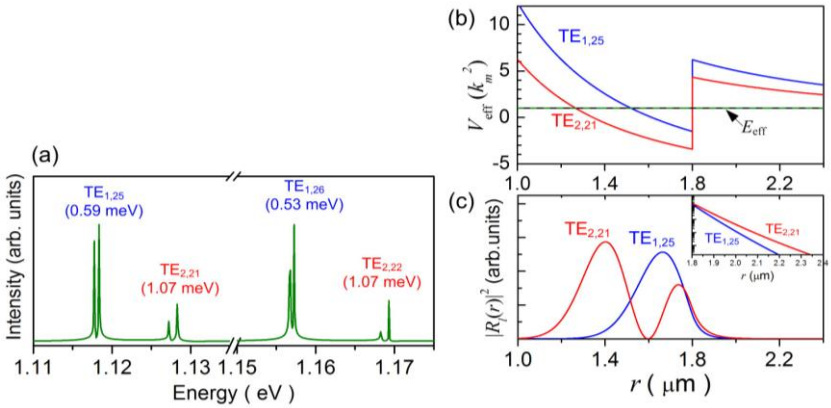

Fig. 5. (a) The 2D FDTD calculations of a PM formed by two identical MDs with 3.6 μm diameters and an inter-gap distance of 75 nm. The numbers marked in brackets are the energy splittings of each WGM pairs. (b) The effective potential, in unit of k_m^2, for the $TE_{1,25}$ and $TE_{2,21}$ modes in a MD with a diameter of 3.6 μm. (c) The field intensities of the $TE_{1,25}$ and $TE_{2,21}$ modes calculated from Eq. (4). The inset shows the field intensities in log scale for the $TE_{1,25}$ and $TE_{2,21}$ modes outside the MDs.

Because n_{eff} changes abruptly at the boundary of the disk-air interface, a discontinuity in V_{eff} occurs at $r = a$, giving rise to a potential well for the field inside the MD, as shown in Fig. 5(b) for the $TE_{1,25}$ and $TE_{2,21}$ modes in a MD with $a = 1.8\,\mu\text{m}$. In this sense, $V_{\text{eff}} - E_{\text{eff}} = (m/a)^2 - (2\pi n_{\text{eff}} / \lambda_m)^2$ defines an effective barrier height for a given mode. Since $m(\lambda_m / 2n_{\text{eff}}) \propto 2\pi a$ due to the standing wave conditions, the effective barrier height will scale as m^2 for a given disk size a. This means that a higher-order azimuthal mode will experience a higher effective barrier and, as a result, have a smaller coupling strength with the adjacent MD due to the less evanescent wave leaked into the MD gap. On the other hand, for WGMs with the same m but different ℓ in a MD, a higher-order radial mode with an inner orbital will experience a lower effective barrier and hence being less confined at the MD edge. For the $TE_{1,25}$ and $TE_{2,21}$ modes shown in Fig. 5(b) as an example, we can see that the effective barrier height for the $TE_{1,25}$ mode is significantly higher than that for the $TE_{2,21}$ mode. Because their resonant wavelengths are quite close, the effective barrier height is mostly determined by the azimuthal mode number m and increases with m^2. The effective barrier heights for the $TE_{1,25}$ and $TE_{2,21}$ modes shown in Fig. 5(b) have a ratio of about 1.57, which is roughly equal to $(25/21)^2 \sim 1.4$ estimated from the ratio of m^2. In Fig. 5(c), the field intensities of the $TE_{1,25}$ and $TE_{2,21}$ modes calculated from Eq. (4) are displayed. As anticipated, the $TE_{2,21}$ mode with an inner orbital is less confined. Thereby, the field intensity of the $TE_{2,21}$ mode outside the MD show a slower decay than that of the $TE_{1,25}$ mode. The analytical calculations illustrated here qualitatively explain why the second-order radial modes ($\ell = 2$) show larger coupling strengths than the adjacent first-order modes ($\ell = 1$).

4. Conclusions and outlook

Strong couplings between whispering-gallery modes in photonic molecules formed by two preselected nearly identical microdisk microcavities have been investigated. Clear anticrossings in the resonant energies associated with crossings in the peak linewidths were observed. Strong coupling can occur not only between identical modes, but also between those with different radial and azimuthal mode numbers. The observed energy anticrossing and the linewidth crossing can be well described by the coupled mode theory, by which the coupling strengths of different modes can be extracted. We found that the coupling strengths

#134575 - $15.00 USD Received 7 Sep 2010; revised 23 Oct 2010; accepted 23 Oct 2010; published 29 Oct 2010

of second-order radial modes ($\ell = 2$) are larger than that of the adjacent first-order radial modes ($\ell = 1$). The physical origin of the different coupling strengths have also been elucidated by the effective barrier for the confined electromagnetic waves in the microdisk. The observed coupling strengths can be up to 0.32 meV ($g/2\pi = 77$ GHz) for the first-order radial mode and 0.86 meV ($g/2\pi = 208$ GHz) for the second-order radial mode. The coupling strengths of optical modes are nearly an order of magnitude higher than the dot-cavity coupling strength (10-30 GHz) that has been realized thus far. If the dot-cavity strong coupling can be further achieved in each microdisk, it is possible to realize a longer-distance coupling between two quantum dots in different locations. However, due to the requirement of spectral and spatial matching between the dot and cavity modes, a very low yield can be expected. Our experimental approach, which allows assembling photonic molecules out of preselected microdisks, combined with techniques of local addressing individual quantum dots and resonant modes in each cavity, may provide a shortcut to this goal. The highly flexible and controllable photonic-molecule systems investigated here are thus very promising for realizing the transfer of quantum information between different quantum dots located in different cavities mediated by the strong photon-field coupling.

Acknowledgement

This work was supported in part by the program of MOE-ATU and the National Science Council of Taiwan under Grant Nos.: NSC-99-2112-M-009-008-MY2.

#134575 - $15.00 USD Received 7 Sep 2010; revised 23 Oct 2010; accepted 23 Oct 2010; published 29 Oct 2010